Medical Physics
The International Journal of Medical Physics Research and Practice

Photoacoustic detection and optical spectroscopy of high-intensity focused ultrasound-induced thermal lesions in biologic tissue

Mosa Alhamami, Michael C. Kolios, and Jahan Tavakkoli

Citation: Medical Physics **41**, 053502 (2014); doi: 10.1118/1.4871621
View online: http://dx.doi.org/10.1118/1.4871621
View Table of Contents: http://scitation.aip.org/content/aapm/journal/medphys/41/5?ver=pdfcov
Published by the American Association of Physicists in Medicine

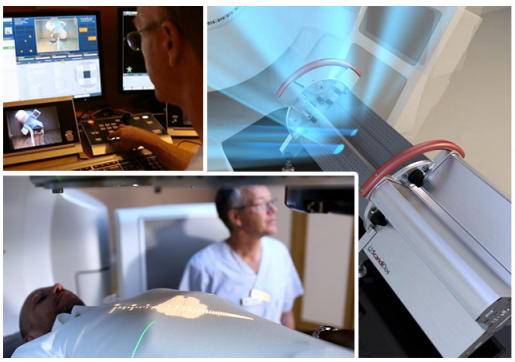

Photoacoustic detection and optical spectroscopy of high-intensity focused ultrasound-induced thermal lesions in biologic tissue

Mosa Alhamami, Michael C. Kolios, and Jahan Tavakkoli[a)]
Department of Physics, Ryerson University, 350 Victoria Street, Toronto, Ontario M5B 2K3, Canada

(Received 7 September 2013; revised 5 February 2014; accepted for publication 3 April 2014; published 24 April 2014)

Purpose: The aims of this study are: (a) to investigate the capability of photoacoustic (PA) method in detecting high-intensity focused ultrasound (HIFU) treatments in muscle tissues *in vitro*; and (b) to determine the optical properties of HIFU-treated and native tissues in order to assist in the interpretation of the observed contrast in PA detection of HIFU treatments.
Methods: A single-element, spherically concaved HIFU transducer with a centre frequency of 1 MHz was utilized to create thermal lesions in chicken breast tissues *in vitro*. To investigate the detectability of HIFU treatments photoacoustically, PA detection was performed at 720 and 845 nm on seven HIFU-treated tissue samples. Within each tissue sample, PA signals were acquired from 22 locations equally divided between two regions of interest within two volumes in tissue – a HIFU-treated volume and an untreated volume. Optical spectroscopy was then carried out on 10 HIFU-treated chicken breast specimens in the wavelength range of 500–900 nm, in 1-nm increments, using a spectrophotometer with an integrating sphere attachment. The authors' optical spectroscopy raw data (total transmittance and diffuse reflectance) were used to obtain the optical absorption and reduced scattering coefficients of HIFU-induced thermal lesions and native tissues by employing the inverse adding-doubling method. The aforementioned interaction coefficients were subsequently used to calculate the effective attenuation coefficient and light penetration depth of HIFU-treated and native tissues in the wavelength range of 500–900 nm.
Results: HIFU-treated tissues produced greater PA signals than native tissues at 720 and 845 nm. At 720 nm, the averaged ratio of the peak-to-peak PA signal amplitude of HIFU-treated tissue to that of native tissue was 3.68 ± 0.25 (mean ± standard error of the mean). At 845 nm, the averaged ratio of the peak-to-peak PA signal amplitude of HIFU-treated tissue to that of native tissue was 3.75 ± 0.26 (mean ± standard error of the mean). The authors' spectroscopic investigation has shown that HIFU-treated tissues have a greater optical absorption and reduced scattering coefficients than native tissues in the wavelength range of 500–900 nm. In fact, at 720 and 845 nm, the ratio of the optical absorption coefficient of HIFU-treated tissues to that of native tissues was 1.13 and 1.17, respectively; on the other hand, the ratio of the reduced scattering coefficient of HIFU-treated tissues to that of native tissues was 13.22 and 14.67 at 720 and 845 nm, respectively. Consequently, HIFU-treated tissues have a higher effective attenuation coefficient and a lower light penetration depth than native tissues in the wavelength range 500–900 nm.
Conclusions: Using a PA approach, HIFU-treated tissues interrogated at 720 and 845 nm optical wavelengths can be differentiated from untreated tissues. Based on the authors' spectroscopic investigation, the authors conclude that the observed PA contrast between HIFU-induced thermal lesions and untreated tissue is due, in part, to the increase in the optical absorption coefficient, the reduced scattering coefficient and, therefore, the deposited laser energy fluence in HIFU-treated tissues.
 [http://dx.doi.org/10.1118/1.4871621]

Key words: high-intensity focused ultrasound (HIFU), thermal lesions, photoacoustic (PA) detection, optical spectroscopy, optical properties of chicken breast tissue

1. INTRODUCTION

High-intensity focused ultrasound (HIFU) is a bloodless surgical modality that is capable of inducing thermal and mechanical effects in deep-seated regions of interest (ROI) selectively and noninvasively.[1] Using a high-power focused transducer, HIFU beams can be achieved and focalized within the transducer's focal zone in order to deposit acoustic energy in the ROI with minimal or no harm to intervening tissue layers. Within the ROI, the selectively deposited acoustic energy is converted into heat, raising the temperature of the targeted tissue volume, while generally keeping the temperature of the surrounding tissue volumes at physiologically safe levels. The increase in the targeted tissue temperature above 56 °C for at least 1 s can lead to immediate cell death due to protein denaturation in a process known as coagulation necrosis.[2] The spatially confined, coagulated tissue volumes are termed thermal lesions,[3] since the predominant mechanism of HIFU is thermal, although cavitation and boiling bubbles are also involved in the formation and

shaping of the induced thermal lesions,[2] particularly at higher temperatures.

HIFU has been explored for various therapeutic applications including, but not limited to, hemostasis,[4,5] neurology and pain management,[6] cosmetic surgery,[7] and ophthalmology.[8,9] Moreover, HIFU therapy demonstrated a great potential for oncological applications including treatments of tumors in the prostate,[10–12] breast fibroadenoma,[13] uterine fibroids,[14,15] kidney,[12,16] liver,[12,17] bladder,[18] bone,[19,20] and brain.[21,22] Oncologic and other applications of HIFU are expected to expand with the development of optimized imaging techniques that can provide real-time HIFU treatment monitoring, evaluation, and control.

Currently, most HIFU treatments are monitored and guided with magnetic resonance imaging (MRI) (Refs. 11, 13, 14, 17, and 19–23) and ultrasound imaging.[24,25] However, the challenges associated with the aforementioned imaging modalities, including cost and equipment compatibility with MRI as well as low contrast-resolution between treated and normal tissues with ultrasound imaging, have stimulated the interest of many research groups to investigate alternative HIFU monitoring tools. Among the proposed techniques is photoacoustic (PA) imaging. It is based on the optical absorption of a short, pulsed laser irradiation and the subsequent generation of acoustic waves. These laser-induced acoustic waves, generated as a result of thermoelastic expansion in the absorbing medium, are detectable by a diagnostic ultrasound transducer.[26] Therefore, PA imaging combines the advantages of both ultrasound and optical imaging modalities, i.e., it provides higher resolution than optical imaging and higher tissue contrast than ultrasound imaging.[26] The higher resolution of PA imaging is due to the weaker ultrasound scattering in tissues than optical scattering.[26] On the other hand, the higher tissue contrast of PA imaging is due to its capability in visualizing the tissue optical absorption properties, providing the advantage of functional imaging of important physiological parameters such as hemoglobin concentration.[26] Moreover, PA imaging is a noninvasive modality that utilizes a nonionizing electromagnetic radiation.

The possibility of PA detection of HIFU-induced thermal lesions has been demonstrated *in vitro*,[27,28] *ex vivo*,[29] and *in vivo*.[30] Moreover, previous studies have also been successful in detecting laser-induced thermal lesions photoacoustically.[31,32] Because the generated PA pressure depends on the absorbed optical energy (i.e., the product of laser energy fluence and optical absorption coefficient) and the thermoacoustic efficiency of the absorbing structure, a change in at least one of these factors can result in a change in the detected PA signal. Therefore, thermally induced changes in the optical[33–36] and thermomechanical[37,38] properties of tissues have been investigated following laser-induced thermotherapy or water/saline-bath heating. However, to our knowledge, the optical and thermomechanical properties of HIFU-treated tissues have not yet been examined in conjunction with PA detection of HIFU treatments. In this work, we demonstrate the possibility of PA detection of HIFU-induced thermal lesions in chicken breast tissues *in vitro* at 720 and 845 nm laser illuminations. Moreover, for the first time, we measure the optical properties (total transmittance, diffuse reflectance, absorption coefficient, reduced scattering coefficient, effective attenuation coefficient, and light penetration depth) of HIFU-induced thermal lesions and compare them with native (untreated) tissues in the wavelength range of 500–900 nm. The aforementioned objectives are intended to test our hypothesis that PA detection of HIFU-induced thermal lesions is feasible due, in part, to changes in the optical properties of HIFU-treated tissues.

2. MATERIALS AND METHODS

2.A. The HIFU transducer and its driving electronics

A single-element, spherically concaved HIFU transducer (6699A101, Imasonic S. A.,Voray-sur-l'Ognon, France) made of a high-power piezocomposite material was used in this study. The transducer had a resonance frequency of 1 MHz, aperture diameter of 125 mm, and radius of curvature of 100 mm. It was calibrated using a needle hydrophone (HNA-0400, ONDA Corporation, Sunnyvale, CA) as well as a radiation force balance unit (RFB-2000, ONDA Corporation, Sunnyvale, CA).[39] The transducer's efficiency (ratio of measured output acoustic power to the net input electric power) was determined to be ∼0.64 (Ref. 39) for the net input electric power used in this study, which was ∼110 W. Based on a numerical simulation of the acoustic field, the HIFU transducer had a depth of field of ∼7.55 mm and a −6 dB focal beam width of 1.24 mm.

The HIFU transducer was driven by an arbitrary function generator (AFG3022B, Tektronix, Beaverton, OR), which generated electrical radiofrequency (RF) signals. An RF power amplifier (A150, Electronics and Innovation, Rochester, NY) was utilized to amplify the generated RF signals. To maximize the transmitted power to the HIFU transducer, a matching network connected the RF power amplifier with the transducer. Moreover, a multilogger thermometer (HH506RA, OMEGA Engineering Inc., Stamford, CT) was used to monitor the change in the HIFU transducer's surface temperature during treatments, thereby ensuring safe operation of the transducer. A schematic diagram of the experimental setup is shown in Fig. 1.

2.B. HIFU treatments

As a biologic tissue model for HIFU treatments, *in vitro* chicken breast tissues, purchased from a local market, were used in this study. For both the PA detection and optical spectroscopy experiments, the tissues were cut into approximately 7.5 cm × 6.5 cm × 1.5 cm (length × width × thickness) samples, and five HIFU thermal lesions were created in each sample by manually moving the tissue holder using a micropositioning controller (Fig. 1) to five different locations separated by 5 mm. The sequence of generating the five HIFU thermal lesions is illustrated in Fig. 2(a). The treated region in each sample, which consisted of five HIFU thermal lesions, is shown in Fig. 2(b).

Operated with 60% duty cycle, the HIFU transducer generated focused waves that propagated through ∼9.0 cm in

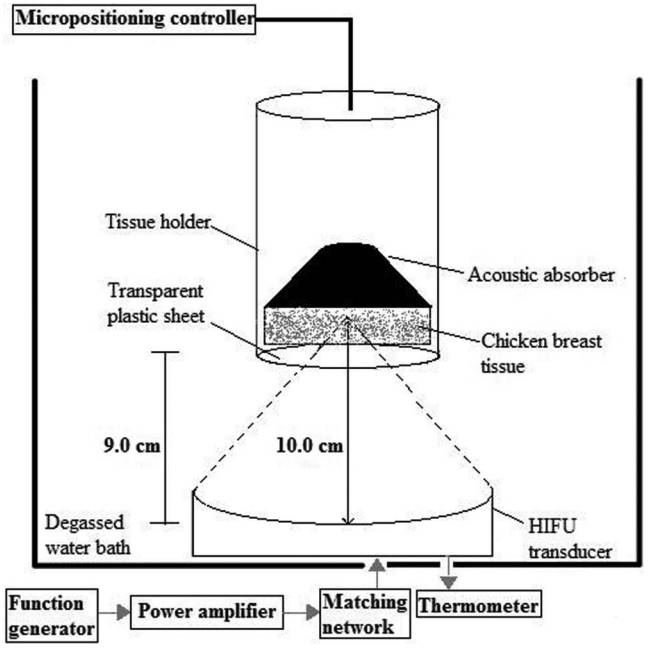

FIG. 1. Schematic diagram of the experimental setup of HIFU treatments. The focus of the HIFU transducer was at 10.0 cm. The distance between the centre of the transducer and the transparent plastic sheet covering the opening of the tissue holder was ∼9.0 cm, resulting in a tissue focal depth of ∼1.0 cm.

degassed water at room temperature (∼20 °C) and 1.0 cm in tissue, creating thermal lesions with acoustic intensity, I_{SPTA}, of ∼1690 W/cm^2 at the transducer's focus inside tissue. The free-field I_{SPTA} was ∼1910 W/cm^2. The transmitted acoustic power in each HIFU treatment was ∼42 W, and the total sonication time was 30 s.

2.C. Photoacoustic detection

2.C.1. The PA system

PA detection of HIFU treatments was achieved using the Imagio Small Animal PA imaging system (Seno Medical Instruments Inc., San Antonio, TX). A schematic diagram of the experimental setup is shown in Fig. 3.

The utilized PA imaging system consisted of a pulsed titanium:sapphire (Ti:Al_2O_3) laser with wavelengths tunable in the range between 720 and 850 nm. Delivered through an articulated arm, the pulsed laser had a 9-mm beam diameter,

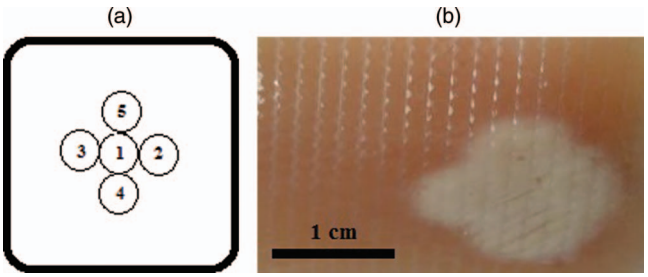

FIG. 2. (a) The sequence followed in creating HIFU thermal lesions. (b) A plastic-wrapped, vacuum-sealed chicken breast tissue sample containing HIFU-treated and native ROIs.

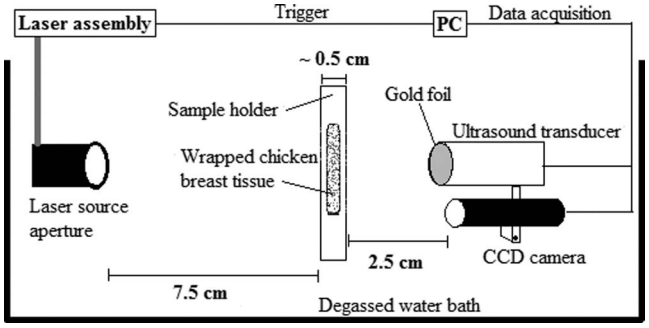

FIG. 3. Schematic diagram of the experimental setup of PA detection. In this diagram, the connection between the laser source aperture and the laser assembly does not depict the actual articulated arm for laser beam delivery.

6-ns pulse width, and 10-Hz pulse repetition rate. The maximum output energy of the laser at the wavelengths used in this study was ∼128 mJ, which corresponds to a maximum laser energy fluence of 201 mJ/cm^2 at the irradiated tissue surface. This energy level causes a thermoelastic expansion and results in strong PA signals from the native and treated chicken breast tissues, although they do not inherently contain very strong light chromophores.

The photoacoustic receiver of the PA imaging system was a 4-element annular array ultrasound transducer with a centre frequency of 5 MHz. The −6 dB bandwidth of the transducer was 60% and its focal length was 29.5 mm, as determined previously.[40] The transducer, which had a depth of field of ∼10 mm, was coaxially mounted at a distance of 105 mm from the laser source in order to allow raster scanning of the chicken breast sample under investigation, which was placed within the transducer's depth of field (Fig. 3). A 52-μm-thick, PVDF-based gold foil (210037022, Measurement Specialities Inc., Hampton, VA) was used to protect the ultrasound transducer from direct laser exposure. Moreover, a charge-coupled device (CCD) camera, placed underneath the ultrasound transducer, was utilized to facilitate targeting of the ROI by the laser beam by providing a real-time view of the target region that is at the cross hair of the laser. The CCD camera is part of the commercial Imagio PA system.

2.C.2. Tissue sample preparation for PA detection

Prior to performing the PA detection experiments, the HIFU-treated chicken breast samples were cut into approximately 4.0 cm × 3.0 cm (width × length) and were sliced to ∼0.5 cm thickness using a professional food slicer (1060-C, The Rival Company, El Paso, TX). Slicing the chicken breast samples eliminated the undesired skin part of the tissue, and reduced the extension of the superficial thermal lesion in the sliced tissue volume to ∼0.35 cm. Moreover, in order to prevent contamination of the water tank, the samples were plastic wrapped and vacuum sealed with a vacuum sealer (V2060 FoodSaver, Jarden Corp., Rye, NY).

2.C.3. PA measurements

The plastic-wrapped, vacuum-sealed samples, shown in Fig. 2(b), were then attached to a tissue holder and placed

within the focal zone of the ultrasound transducer inside the PA imaging system's water reservoir (Fig. 3). To compare the PA response of HIFU-treated and native tissues, two ROIs were identified in each one of the seven samples examined in this study. One of the ROIs was within a HIFU-treated tissue volume, while the other ROI was within a native tissue volume in the sample under investigation. Horizontal raster scanning was performed with 0.1 mm scan resolution covering 11 locations within each ROI. The laser fired four pulses at each location in the ROI and the detected PA RF signals, which were collected within 0.4 s, were averaged to generate a single PA RF line. Therefore, a total of 11 PA RF lines, obtained from 11 locations, were recorded for each ROI within each sample. The acquired PA data were imported to MATLAB (R2012b, The MathWorks Inc., Natick, MA) for processing. For each one of the seven samples, the 11 PA RF lines were averaged, producing a single PA RF line that corresponds to a particular ROI (treated or native) within that sample. This averaging method was performed since the samples were well-controlled and stable, i.e., they did not produce large variations in space or time within the examined regions. The PA detection experiments were performed with two laser wavelengths: 720 and 845 nm, thereby covering the maximum range of wavelengths generated by our PA imaging system.

It is noteworthy to mention that the PA detection experiments were conducted after assessing the accuracy of the CCD camera in targeting the position of an ROI (Fig. 3) using carbon rods, which are known to produce very strong PA signals. Based on the strength of the acquired PA signals, this testing allowed us to make subtle adjustments in the position of the CCD camera so that the ROI, shown in the real-time CCD camera's image, was coincident with the area that was irradiated by the laser beam.

2.D. Optical spectroscopy

Optical spectroscopy experiments were conducted in this study in order to understand the influence of HIFU-induced changes in the optical properties on the detected PA pressure rise, $\Delta P(z)$. The PA pressure rise is directly proportional to the absorbed optical energy and the thermoacoustic efficiency, and is given in the equation below:[41,42]

$$\Delta P(z) = \Gamma E_{abs}(z) = \Gamma \mu_a \Psi(z), \tag{1}$$

where Γ is the dimensionless Grüneisen parameter, which represents the fraction of thermal energy that is converted into acoustic waves (also known as thermoacoustic efficiency). In Eq. (1), the absorbed optical energy from a laser source, $E_{abs}(z)$ [J/m^3], is the product of the optical absorption coefficient, μ_a [m^{-1}], and the laser energy fluence, $\Psi(z)$ [J/m^2].

Our spectroscopic investigation included measurements of diffuse reflectance (DR) and total transmittance (TT) of chicken breast tissue slices, prepared as described in Sec. 2.D.1, using a commercially available spectrophotometer with an integrating sphere attachment (Sec. 2.D.2). The inverse adding-doubling method, described in Sec. 2.D.3, was utilized to determine the optical absorption coefficient, μ_a, and the reduced scattering coefficient, μ'_s, from the experimental data of the DR and TT. The effective attenuation coefficient, μ_{eff}, and the effective light penetration depth, D_{eff}, were calculated in the wavelength range of 500–900 nm using the following equations:[41]

$$\mu_{eff} = \sqrt{3\mu_a(\mu_a + \mu'_s)}, \tag{2}$$

$$D_{eff} = \frac{1}{\mu_{eff}}. \tag{3}$$

2.D.1. Tissue sample preparation for optical spectroscopy

A new set of chicken breast tissues treated with HIFU, as described in Sec. 2.B, were stored at low temperatures (6–8 °C) for 12–48 h prior to conducting optical spectroscopy experiments. Using the food slicer mentioned in Sec. 2.C, the tissues were sliced to thin slices; each containing HIFU-treated and native tissue regions. The sliced tissue specimens were further trimmed with a knife to fit within a 1-mm spacing between two 1-mm-thick optical glass slides (BK7, Esco Optics Inc., Oak Ridge, NJ), which were spaced apart using stainless steel shims. Sandwiching sliced tissue specimens within the two optical glass slides reduced the tissue surface irregularities. The tissue specimen and the two optical glass slides covering it had a combined thickness of ~3 mm, as measured using a micrometer. Figure 4 is a photograph of one of the 10 sliced tissue specimens that were prepared during our optical spectroscopy experiments.

2.D.2. Integrating-sphere measurements

To compare the optical properties of HIFU-treated and native tissues, the sliced tissue specimens, which were positioned between two optical glass slides, were used in optical spectroscopy experiments using the Shimadzu spectrophotometer (UV 3600 UV-VIS-NIR, Shimadzu Scientific Instruments, Columbia, MD) with the ISR-3100 integrating sphere attachment. The system's sphere diameter was 60.0 mm, entrance port diameter was 16.7 mm, and the exit port diameter was 18.8 mm. The integrating-sphere method allowed us carry out the DR and TT measurements in a

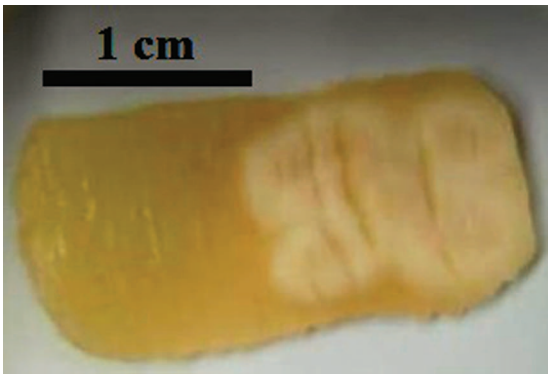

FIG. 4. An approximately 1-mm-thick slice of a chicken breast tissue, containing HIFU-treated and native ROIs, used in the optical spectroscopy experiments.

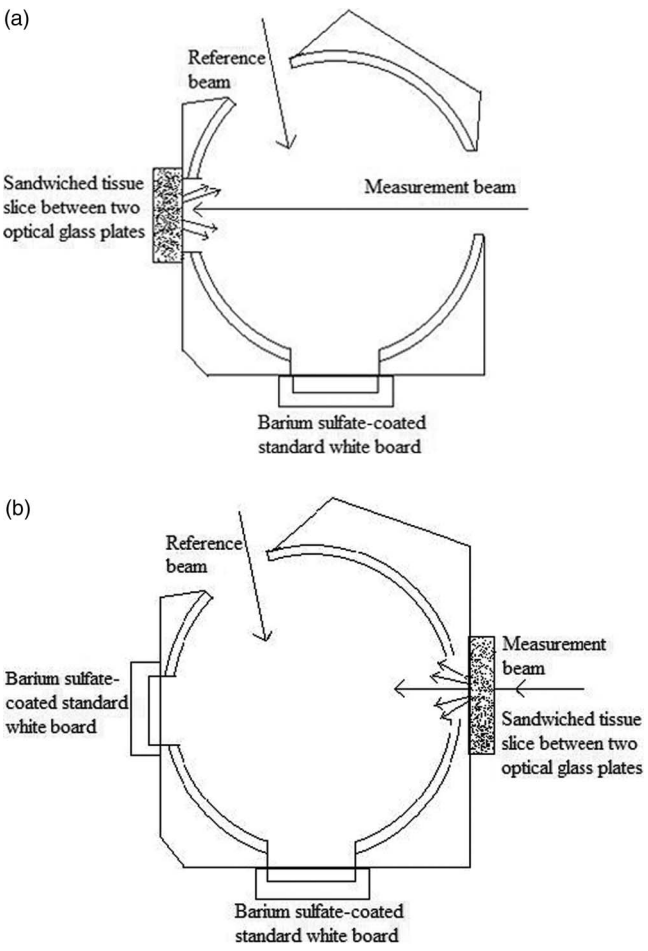

FIG. 5. Diagrams of (a) a dual-beam diffuse reflectance measurement, and (b) a dual-beam total transmittance measurement. The diagrams are reproduced, with permission, from Refs. 43 and 44; courtesy of the Shimadzu Corporation.

dual-beam mode, with a single-integrating-sphere configuration. The utilized slit width, which was fixed during the experiments, was 8 nm, yielding a measured illumination beam of approximately 7.1 mm at the sample surface. The wavelength of grating and detector changes was set at 910 nm. The experimental setup of the DR and TT measurements is depicted in Fig. 5, which was reproduced, with permission, from Shimadzu Corporation.[43,44]

A total of 10 sliced tissue specimens were prepared as described in Sec. 2.D.1. For each one of the 10 sliced tissue specimens, the DR and TT of native and HIFU-treated portions of the tissue were measured three times between 500 and 900 nm in 1-nm increments. Therefore, for a given sliced tissue specimen, four spectra were generated, each of which was an average of three trials. These spectra were: (a) TT and DR for the native portion of a specimen (two spectra), and (b) TT and DR for the HIFU-treated portion of a specimen (two spectra).

2.D.3. Inverse adding-doubling method

The inverse adding-doubling (IAD) program[45,46] was employed in this study to determine the optical absorption and the reduced scattering coefficients of HIFU-treated and native chicken breast tissues using the DR and TT data, collected as described in Sec. 2.D.2. In the IAD program, optical parameters such as scattering, absorption, and scattering anisotropy can be determined by repeatedly solving the radiative transport equation (RTE) until a match with the measured reflection and transmission values is made.[45] The "inverse" implies a reversal to the regular extraction of transmission and reflection values from the optical properties, whereas "adding-doubling" refers to the utilized methodology in solving the RTE.[45] The IAD is a versatile method, and is well-suited for measurements employing biologic tissue specimens positioned between optical glass slides.[45]

2.E. Monte Carlo simulation of light distribution

The light transport in chicken breast tissue was simulated using a Monte Carlo (MC) method developed by Boas *et al.*[47] and modified by Saiko *et al.*[48]. To precisely simulate the light distribution in the tissue, a total of 1×10^8 photons were launched at 720 nm. The tissue was modeled as a box with dimensions 40 mm × 30 mm × 5 mm, while the HIFU-induced thermal lesion was modeled as a cylinder with a diameter of 10 mm and a length of 3.5 mm. The MC simulation allowed us to estimate the light fluence in a native chicken breast tissue slab (i.e., a slab without a lesion) and in another chicken breast tissue slab containing a HIFU-induced thermal lesion, using the measured values of the reduced scattering and absorption coefficients (Fig. 10) at 720 nm. The anisotropy factor, g, was kept constant throughout the simulation ($g = 0.9$).[49] The scattering coefficient, $\mu_s = \mu'_s/(1 - g)$, values used in the MC simulation for a native chicken breast tissue and a HIFU-induced thermal lesion were 2.95 and 39.06 mm^{-1}, respectively. The optical absorption coefficient values, which were extracted directly from Fig. 10(a), used in the MC simulation for a native chicken breast tissue and a HIFU-induced thermal lesion were 0.10 and 0.12 mm^{-1}, respectively. The laser beam diameter used in the simulation was 9 mm.

3. RESULTS AND DISCUSSION

3.A. PA detection of HIFU-induced thermal lesions

Figures 6 and 7 show the PA RF signals of seven samples at 720 and 845 nm laser illumination, respectively, averaged from 11 locations within each ROI in the HIFU-treated and native tissue volumes of each sample. The numerical values that appear inside the rectangular boxes placed within each one of the 14 PA RF lines of Figs. 6 and 7 represent the ratio of the peak-to-peak PA signal amplitudes of HIFU-treated and native ROIs of their respective sample-wavelength combination. Combining the ratios of the seven samples investigated at 720 nm, the averaged ratio of the peak-to-peak PA signal amplitude of HIFU-treated tissue to that of native tissue is 3.68 ± 0.25 (mean ± SEM). At 845 nm, the averaged ratio of the peak-to-peak PA signal amplitude of HIFU-treated tissue to that of native tissue is 3.75 ± 0.26 (mean ± SEM). Figure 8 provides a comparison of the averaged ratios of the HIFU-treated and native tissue peak-to-peak PA signal

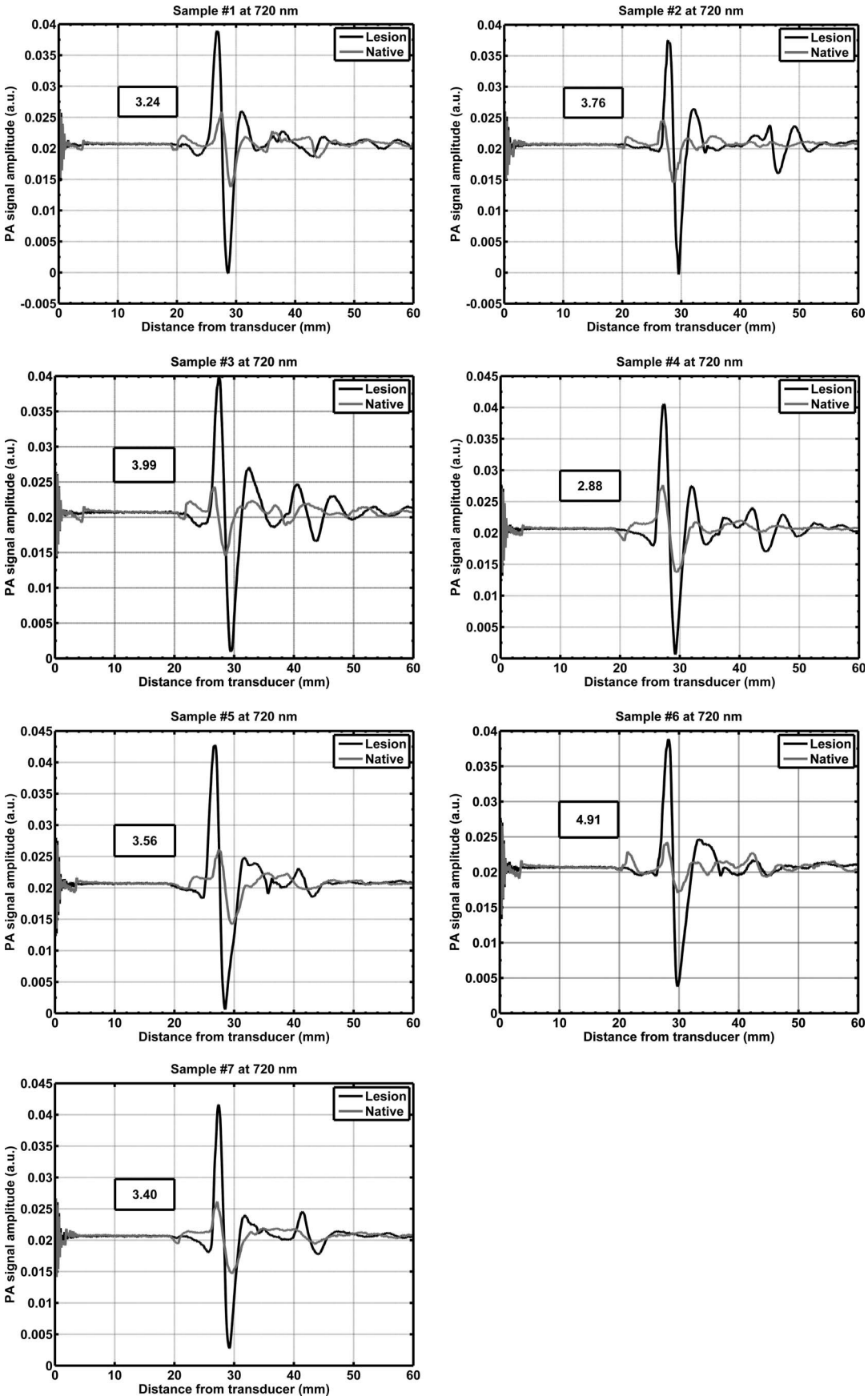

FIG. 6. Photoacoustic RF lines obtained from seven chicken breast samples irradiated at 720 nm. Within a given sample, the lesion and native RF lines represent the average of the RF lines collected at 11 locations within a HIFU-treated and native ROIs, respectively. The numerical values inside the boxes represent the ratio of the averaged peak-to-peak signal amplitudes of HIFU-treated and native ROIs of their respective samples.

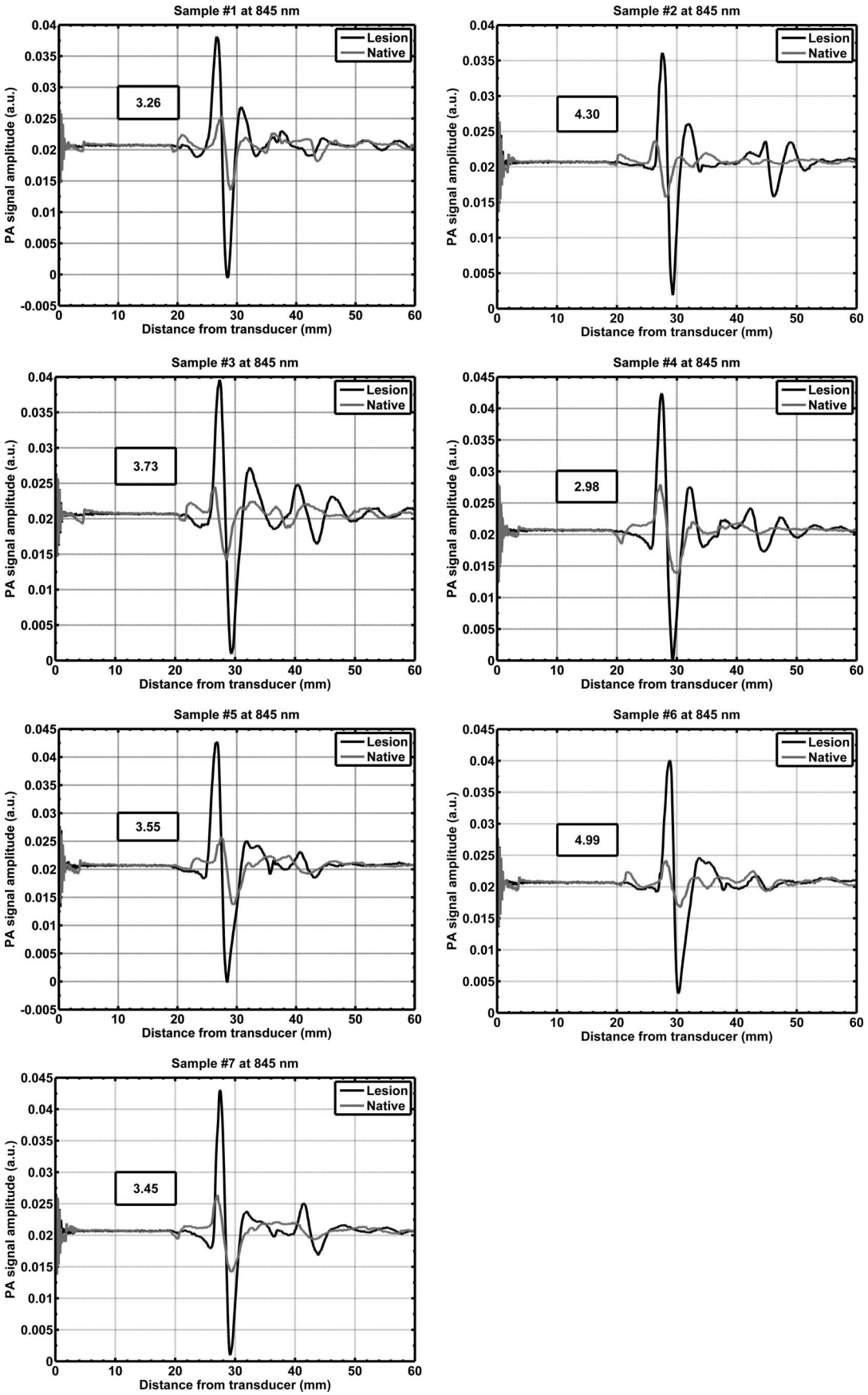

FIG. 7. Photoacoustic RF lines obtained from seven chicken breast samples irradiated at 845 nm. Within a given sample, the lesion and native RF lines represent the average of the RF lines collected at 11 locations within a HIFU-treated and native ROIs, respectively. The numerical values inside the boxes represent the ratio of the averaged peak-to-peak signal amplitudes of HIFU-treated and native ROIs of their respective samples.

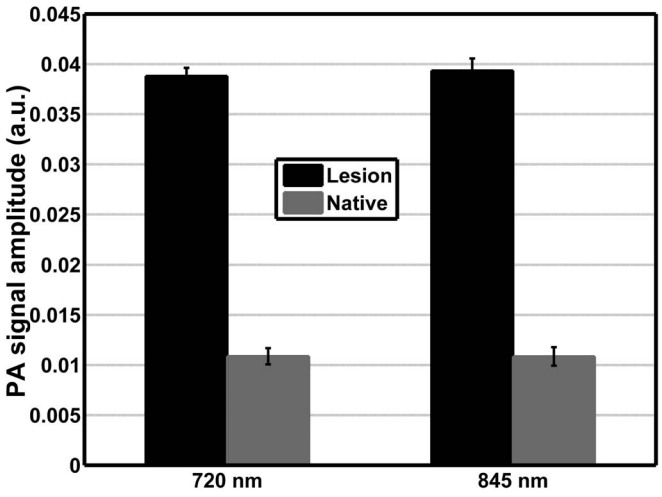

FIG. 8. A comparison between averaged ratios of HIFU-treated and native tissue peak-to-peak PA signal amplitudes from the seven samples obtained at 720 and 845 nm laser illumination. Error bars represent the standard error of the mean (SEM).

amplitudes from the seven samples at 720 and 845 nm laser illumination. The increase in the PA signal amplitude by more than three times as a result of HIFU-induced coagulation has also been reported in a previous study.[28]

In Figs. 6 and 7, the slight shift and, in some cases, the differences in the width of the N-shapes of the PA signals of native and HIFU-treated tissues can be attributed to minor nonuniformity in the surface of the tissue samples used in the PA detection experiments. In few instances, the HIFU-induced thermal lesion appeared as a "bulging mass" that is thicker than the surrounding native tissue, making some of the N-shapes in Figs. 6 and 7 to appear of slightly different widths in native tissues compared to HIFU-induced thermal lesions. It is also important to note that HIFU-induced thermal lesions have a higher acoustic attenuation coefficient than native tissues.[50,51] Therefore, laser-generated PA pressure waves should undergo a greater acoustic attenuation as they propagate through a thermal lesion compared to native tissue. The effect of the increased ultrasound attenuation is expected to be more pronounced in the PA detection geometry of Fig. 3, for which the laser source aperture and the ultrasound transducer are on opposite ends of the sample. Nevertheless, the detected PA signals from HIFU-induced thermal lesions had greater peak-to-peak amplitudes than native tissues. The observed PA contrast between HIFU-treated and native tissues implies that the PA method can indeed detect HIFU-induced thermal lesions at 720 and 845 nm laser illuminations. An understanding of how the detected PA pressure [Eq. (1)] is influenced by HIFU-induced changes in the optical properties is necessary in order to explain the observed PA contrast in Figs. 6 and 7.

3.B. Optical spectroscopy of HIFU-treated and native tissues

3.B.1. Diffuse reflectance and total transmittance

Figure 9 shows the averaged results of the integrating-sphere measurements on 10 chicken breast tissue slices. In Figs. 9(a) and 9(b), the TT and DR spectra are presented,

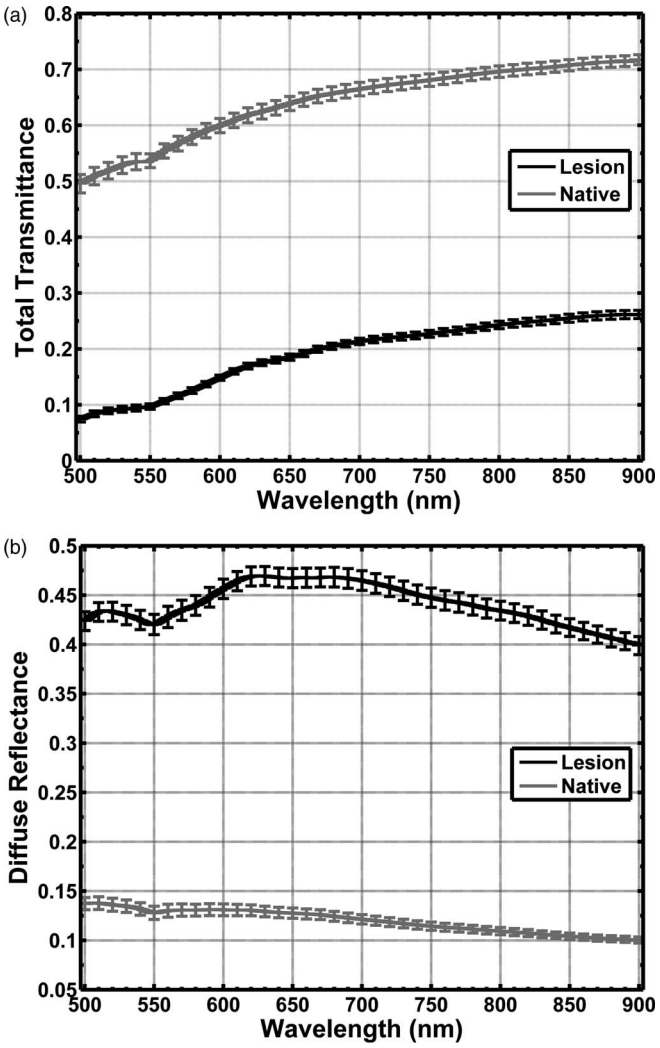

FIG. 9. Results of the integrating-sphere measurements. (a) and (b) show the averaged total transmittance and diffuse reflectance with the SEM, respectively, of HIFU-treated and native tissues in the wavelength range of 500–900 nm.

respectively, with the SEM for both HIFU-treated and native tissues in the wavelength range of 500–900 nm. The TT and DR results provide a quantitative comparison between HIFU-treated and native tissues in terms of their wavelength-dependent ability to reflect and transmit light between 500 and 900 nm. Figure 9(a) shows that the ratio of TT of native tissue to that of HIFU-treated tissue ranges from 5.54 to 6.66 in the wavelength range of 500–550 nm. However, this ratio tends to gradually decrease as the wavelength increases, reaching a value of 2.74 at 900 nm. Figure 9(b) shows that the ratio of DR of HIFU-treated tissue to that of native tissue increases from about 3.09 at 500 nm to about 3.97 at 900 nm. Figures 9(a) and 9(b) show that the wavelength range of 630–900 nm is appropriate for optical diagnostics of HIFU-treated and native chicken breast tissues *in vitro* because light has a relatively high transmittance and low reflectance in this range. This observation will be confirmed later with the effective light penetration depth graph.

3.B.2. Optical absorption and reduced scattering coefficients

Using the IAD program,[46] the optical absorption coefficient and the reduced scattering coefficient spectra were determined for each one of the 10 tissue slices. Figures 10(a) and 10(b) show the averaged optical absorption coefficient and the reduced scattering coefficient spectra, respectively, with the SEM for both HIFU-treated and native tissues in the wavelength range of 500–900 nm. Figure 10(a) shows that the optical wavelength range of approximately 670–900 nm has the lowest absorption coefficient for HIFU-treated and native chicken breast tissue, making it an appropriate range for optical diagnostics of relatively deep-seated ROIs. As per Eq. (1), the difference in the optical absorption coefficients of HIFU-treated and native tissues in the aforementioned optical wavelength range is a contributor to the difference in the PA response detected from HIFU-treated and native tissues at 720 and 845 nm. In other words, the HIFU-induced increase in the PA signal amplitudes (Figs. 6 and 7) can be attributed, in part, to the increased optical absorption coefficients of HIFU-treated tissues as compared to native tissues. Figure 10(b) shows the large difference between the reduced scattering coefficients of HIFU-treated and native tissues. In fact, at 500 nm, the ratio of the reduced scattering coefficients of HIFU-treated tissue to that of native tissue is ~11.19, while at 900 nm the ratio increases to about 15.42. The general decrease in the reduced scattering coefficient spectra of both HIFU-treated and native tissues with wavelength, as depicted in Fig. 10(b), is consistent with a previous work that utilized saline-bath heating of tissues.[36] Although they did not use HIFU treatments in their investigation, Yaroslavsky *et al.*[36] obtained results that are consistent with our result as they have also reported a thermally induced increase in μ_a and μ'_s of saline-bath-treated brain tissues, compared with native brain tissues.[36]

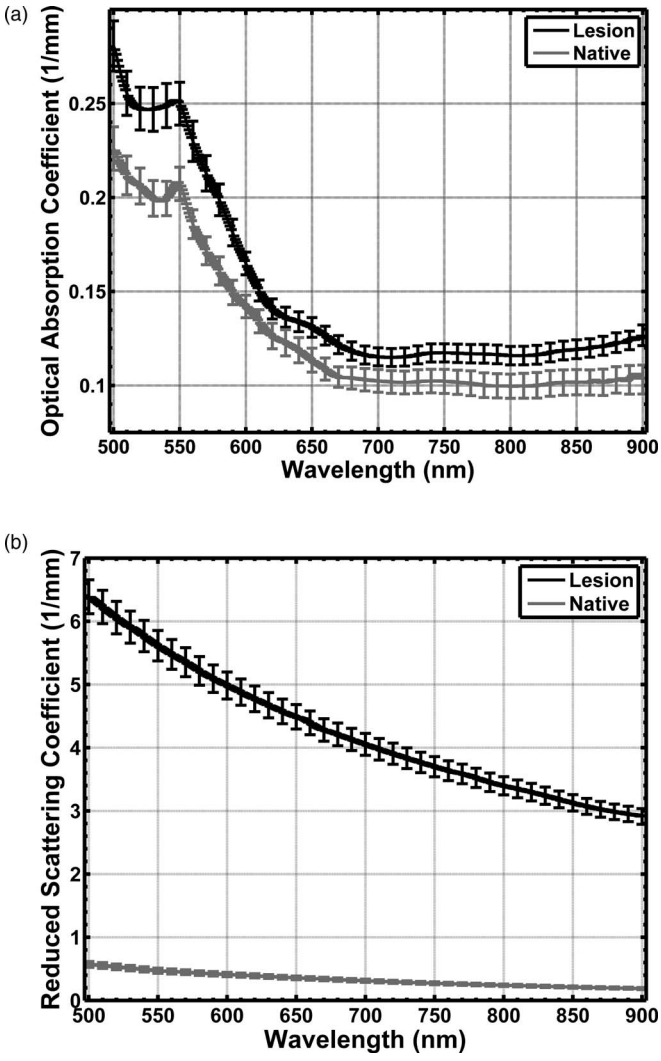

FIG. 10. Results of the IAD computations. (a) and (b) show the averaged optical absorption coefficients and reduced scattering coefficients with the SEM, respectively, of HIFU-treated and native chicken breast tissues in the wavelength range of 500–900 nm.

The observed increase in μ_a of HIFU-treated tissues [Fig. 10(a)] may be attributable, in part, to the thermally induced formation of methemoglobin, a form of hemoglobin with its iron being in the ferric oxidation state, in the blood.[52] The formation of methemoglobin results in an enhanced optical absorption coefficient of the thermally coagulated blood,[52] as compared to native blood, within the wavelength range investigated in our study. Similarly, the increase in μ'_s of HIFU-treated tissue may be explained by the increase in μ'_s of thermally coagulated blood compared to native blood.[52] It is noteworthy to mention that the visual appearance of the chicken breast tissues (i.e., their pink color) as well as their optical absorption spectrum, which resembles that of blood,[53] attest to the presence of hemoglobin in our samples. A similar argument about the presence of blood residuals in excised tissue samples was made in previous studies that utilized liver[27] and brain[36] tissues. However, due to the low blood content in our tissue samples, the thermally induced formation of methemoglobin might not have had a major contribution to the HIFU-induced changes in the optical properties of the tissue samples. Other factors, discussed in the next paragraph, might have resulted in greater changes in the optical properties. These factors include protein coagulation and dehydration (i.e., water loss).

Protein coagulation and dehydration might have been major reasons behind the changes in the optical properties of HIFU-treated tissues. First, thermal denaturation, which causes functional and structural alterations in the heated proteins, results in the production of highly scattering, amorphous granules to replace well-structured, highly organized molecules, present prior to heating.[54] The appearance of the small, thermally denatured granular proteins may be a key factor in the increase in the reduced scattering coefficient of thermally coagulated tissues, based on analyses relying on Mie theory.[55] Second, dehydration and tissue shrinkage have been shown to increase the optical absorption coefficient of biologic tissues.[56] Moreover, by the virtue of decreasing the overall coagulated tissue volume, dehydration and tissue shrinkage may also result in an increase in the concentration of optical attenuators (scattering and absorbing centres).[36] Therefore, HIFU-induced dehydration of the treated tissue

volume can be an important contributor to the increased optical scattering and absorption of the HIFU-induced thermal lesions in the wavelength range investigated in our experiments.

3.B.3. Effective attenuation coefficient and light penetration depth

Using Eqs. (2) and (3), the wavelength-dependent effective attenuation coefficients and light penetration depths were determined, respectively, for each one of the 10 chicken breast tissue slices. Figures 11(a) and 11(b) show the averaged effective attenuation coefficient and the averaged light penetration depth graphs, respectively, with the SEM for both native and HIFU-treated tissues in the wavelength range of 500–900 nm. The gradual decrease in the effective attenuation coefficient and the increase in the effective light penetration depth between 630 and 900 nm in Figs. 11(a) and 11(b), respectively, attest to our previous statement about this range being well-suited for *in vitro* optical diagnostics of HIFU-treated and native chicken breast tissues.

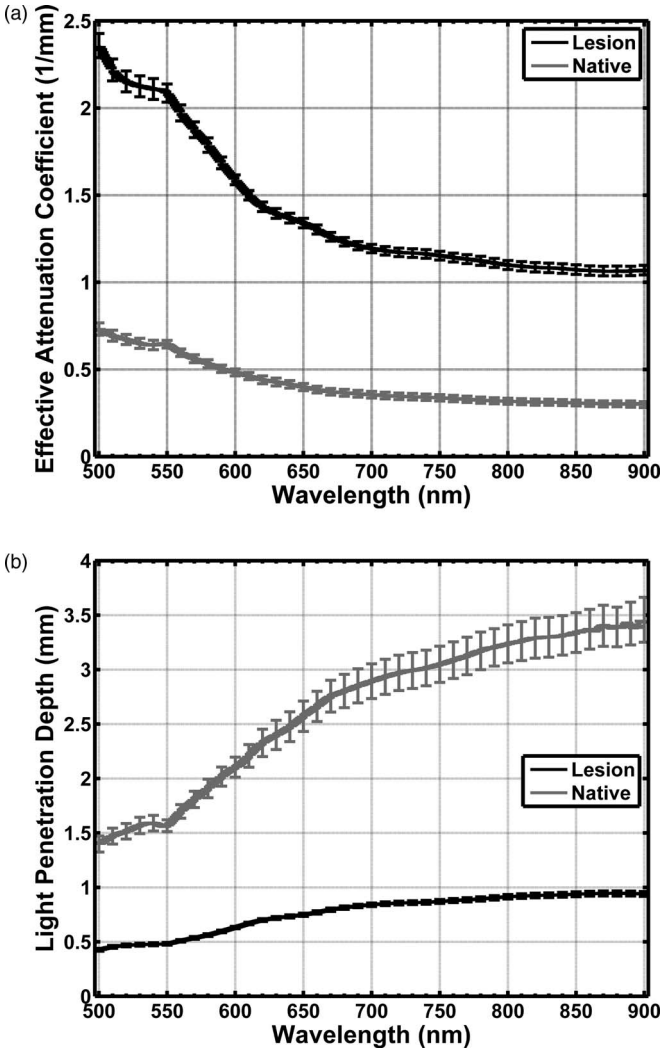

FIG. 11. Results of applying Eqs. (2) and (3). (a) and (b) show the averaged effective attenuation coefficient and effective light penetration depth graphs with the SEM, respectively, of HIFU-treated and native chicken breast tissues in the wavelength range of 500–900 nm.

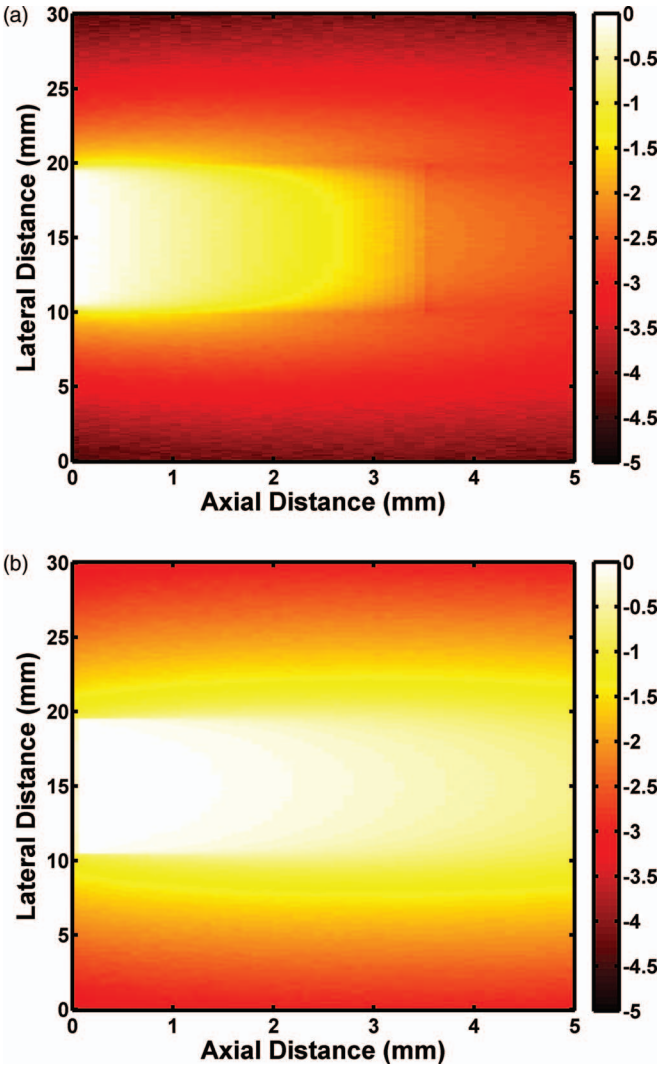

FIG. 12. The results of MC simulation of light distribution in chicken breast tissue. (a) and (b) represent the normalized fluence in a 5-mm-thick slab of tissue with and without a HIFU-induced thermal lesion, respectively. The data are represented in log scale.

Comparing the effective attenuation coefficient and the light penetration depth of HIFU-treated and native tissues can provide an explanation as to why the averaged PA signal amplitudes detected from HIFU-treated tissues were greater than those of native tissues. A superficial HIFU-induced thermal lesion with a lower light penetration depth (i.e., higher effective attenuation coefficient) attenuates greater amount of the incident laser energy than a superficial native tissue of the same volume. In other words, within a HIFU-treated tissue volume, there is a greater probability of photon interactions than a native tissue of the same volume, reducing the light penetration depth and increasing its propagation duration inside the coagulated tissue. Consequently, the amount of the laser energy that is deposited within a HIFU-treated tissue is greater than that within a native tissue, producing a stronger PA pressure rise due to an increase in the laser energy fluence [Eq. (1)].

In summary, within the volume of a HIFU-induced thermal lesion, there are greater light-tissue interactions

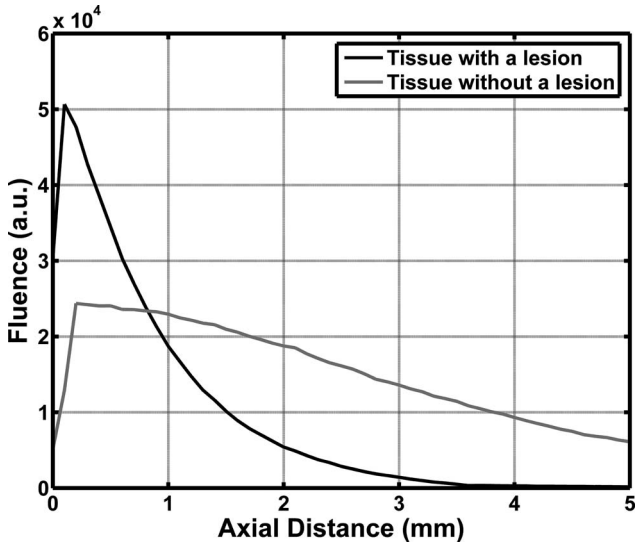

FIG. 13. Comparison of light fluence as a function of axial distance (depth) in chicken breast tissue with and without a HIFU-induced thermal lesion. The graph represents the unnormalized fluence along the z-axis at the centerline (i.e., lateral distance = 15 mm) of Fig. 12.

(scattering and absorption) that decrease the effective light penetration depth and confine most of its energy (i.e., increase laser fluence) within the lesion's volume, thereby producing greater PA signal amplitudes than native tissues.

3.C. Monte Carlo simulation of light distribution

The 2D normalized photon fluence within a 5-mm-thick slab of tissue is shown in Figs. 12(a) and 12(b) for a chicken breast with and without a HIFU-induced thermal lesion, respectively. Figure 13 shows the unnormalized photon fluence along the axial distance (z) of the tissue at the centerline (i.e., lateral distance = 15 mm) of Fig. 12. Because the tissue optical properties, and thus light distribution, do not dramatically change between 720 and 845 nm, the MC simulation results are shown for the case when the laser illumination is at 720 nm. These results provide a quantitative confirmation to our aforementioned statement about the confinement of laser energy within the volume of the thermal lesion due to the increased light-tissue interactions and the reduced effective light penetration depth (Fig. 11), resulting in an increased photon fluence by ~2.23-fold in the thermal lesion at and very close ($z \leq 0.8$ mm) to the tissue surface, as shown in Fig. 13. We believe that this increase in the photon fluence is a factor contributing to the increase in the PA signal amplitudes of HIFU-treated tissues.

It should be noted that in Fig. 12(a) at axial distance of 3.5 mm, where the boundary between the native and the HIFU-coagulated tissues is located, a vertical discontinuity appears as a result of a sudden change in the scattering coefficient of tissue, causing a sudden change in the mean free path of photons.

4. CONCLUSIONS

In this study, we have successfully demonstrated the feasibility of PA detection of HIFU-induced thermal lesions in chicken breast tissues *in vitro* at 720 and 845 nm laser illuminations. A more than threefold increase was observed in the PA signal amplitudes of HIFU-treated tissues compared to native (i.e., untreated) tissues at 720 and 845 nm optical wavelengths, indicating that PA method is indeed capable of detecting HIFU-induced tissue coagulation necrosis and its associated alterations in the molecular and structural compositions of tissues. In order to assist in the interpretation of the aforementioned PA contrast between HIFU-treated and native tissues, we have determined, for the first time, the optical properties of HIFU-induced thermal lesions and compared them with native tissues by performing optical spectroscopy in the wavelength range of 500–900 nm. Based on Eq. (1), our spectroscopic investigation has shown that there are direct and indirect optical factors that together contributed to the observed enhancement in the PA pressure as a result of HIFU-induced thermal lesions. The direct optical factor is the increase in the optical absorption coefficient of the HIFU-treated tissue. The indirect optical factor is the large increase in the reduced scattering coefficient, which contributed to an increase in the effective optical attenuation coefficient and a decrease in the light penetration depth. Hence, the increase in the reduced scattering coefficient has indirectly enhanced the PA pressure rise by increasing the absorbed optical energy [Eq. (1)]. For a complete analysis of the effects of the parameters in Eq. (1) on the detected PA pressure, assessment of the contribution of thermoacoustic efficiency (Grüneisen parameter) of HIFU-induced thermal lesions on the detected pressure rise should be studied in biologic tissues. Based on the results in Figs. 10(a) and 13, from which we determined an approximately 1.13- and 2.23-fold increase in the optical absorption coefficient and photon fluence, respectively, it is expected, based on Eq. (1), that the HIFU-induced thermal lesion had a ~1.46-fold increase in the Grüneisen parameter compared to native tissue, producing a PA signal amplitude increase of about 3.68 at 720 nm. It is also suggested to extend this work to a more clinically relevant scenario by using an *in vivo* animal model. The blood content in *in vivo* animal models will have an important role on the generated PA signals from HIFU-treated and native tissues. If methemoglobin is formed in the blood,[30] it is anticipated that the generated PA signals could have greater amplitudes for HIFU-treated tissues compared to native tissues because of the reasons discussed in Sec. 3.B.2. On the other hand, if methemoglobin is not formed in the blood, it is expected, as shown in a previous work,[30] that HIFU-induced thermal coagulation could potentially result, depending on the optical illumination wavelength, in a reduction in the PA signal amplitude in regions where there is a large amount of blood, particularly due to reduction of blood plasma and the coagulation of red blood cells in the HIFU-treated region.

The main limitation in this study is the offline detection of HIFU-induced thermal lesions. This was caused by the limited geometry and physical dimensions of the utilized PA imaging system, which did not allow us to combine both HIFU and PA imaging together, although such a combination is possible in principle. For real-time PA imaging and monitoring of HIFU treatments, it is suggested to

build a system that combines both HIFU and PA imaging subsystems.

ACKNOWLEDGMENTS

The authors would like to thank Dr. Alexandre Douplik for fruitful discussions during this project. Arthur Worthington, Aditya Pandya, Martin Hohmann, and Eno Hysi are gratefully acknowledged for assistance and technical support. This work was partially supported by the Ontario Research Fund-Research Excellence (ORF-RE) grant and the Natural Sciences and Engineering Research Council of Canada (NSERC Discovery grant) that were awarded to Dr. J. Tavakkoli and Dr. M. C. Kolios. A Natural Sciences and Engineering Research Council of Canada Research Tools and Instrumentation (RTI) grant awarded to Dr. M. C. Kolios supported the purchase of the Shimadzu spectrophotometer used in this study.

[a]Author to whom correspondence should be addressed. Electronic mail: jtavakkoli@ryerson.ca

[1]S. Vaezy, M. Andrew, P. Kaczkowski, and L. Crum, "Image-guided acoustic therapy," Annu. Rev. Biomed. Eng. **3**, 375–390 (2001).
[2]C. R. Hill and G. R. ter Haar, "High intensity focused ultrasound – Potential for cancer treatment," Br. J. Radiol. **68**, 1296–1303 (1995).
[3]G. ter Haar and C. Coussios, "High intensity focused ultrasound: Physical principles and devices," Int. J. Hyperthermia **23**, 89–104 (2007).
[4]S. Vaezy, R. Martin, P. Kaczkowski, G. Keilman, B. Goldman, H. Yaziji, S. Carter, M. Caps, and L. Crum, "Use of high-intensity focused ultrasound to control bleeding," J. Vasc. Surg. **29**, 533–542 (1999).
[5]S. Vaezy *et al.*, "Liver hemostasis using high-intensity focused ultrasound," Ultrasound Med. Biol. **23**, 1413–1420 (1997).
[6]J. L. Foley, S. Vaezy, and L. A. Crum, "Applications of high-intensity focused ultrasound in medicine: Spotlight on neurological applications," Appl. Acoust. **68**, 245–259 (2007).
[7]W. White, I. Makin, P. Barthe, M. Slayton, and R. Gliklich, "Selective creation of thermal injury zones in the superficial musculoaponeurotic system using intense ultrasound therapy: A new target for noninvasive facial rejuvenation," Arch. Facial Plastic Surgery **9**, 22–29 (2007).
[8]D. Coleman, F. Lizzi, J. Driller, A. Rosado, S. Chang, T. Iwamoto, and D. Rosenthal, "Therapeutic ultrasound in the treatment of glaucoma. I. Experimental model," Ophthalmology **92**, 339–346 (1985).
[9]D. Coleman, F. Lizzi, J. Driller, A. Rosado, S. Burgess, J. Torpey, M. Smith, R. Silverman, M. Yablonshi, and S. Chang, "Therapeutic ultrasound in the treatment of glaucoma. II. Clinical applications," Ophthalmology **92**, 347–353 (1985).
[10]J. Chapelon, M. Ribault, F. Vernier, R. Souchon, and A. Gelet, "Treatment of localized prostate cancer with transrectal high intensity focused ultrasound," Eur. J. Ultrasound **9**, 31–38 (1999).
[11]W. A. N'djin, M. Burtnyk, I. Kobelevskiy, S. Hadjis, M. Bronskill, and R. Chopra, "Coagulation of human prostate volumes with MRI-controlled transurethral ultrasound therapy: Results in gel phantoms," Med. Phys. **39**, 4524–4536 (2012).
[12]A. G. Visioli, I. H. Rivens, G. R. ter Haar, A. Horwich, R. A. Huddart, E. Moskovic, A. Padhani, and J. Glees, "Preliminary results of a phase I dose escalation clinical trial using focused ultrasound in the treatment of localised tumours," Eur. J. Ultrasound **9**, 11–18 (1999).
[13]K. Hynynen, O. Pomeroy, D. N. Smith, P. E. Huber, N. J. McDannold, J. Kettenbach, J. Baum, S. Singer, and F. A. Jolesz, "MR imaging-guided focused ultrasound surgery of fibroadenomas in the breast: A feasibility study," Radiology **219**, 176–185 (2001).
[14]C. M. C. Tempany, E. A. Stewart, N. McDannold, B. J. Quade, F. A. Jolesz, and K. Hynynen, "MR imaging-guided focused ultrasound surgery of uterine leiomyomas: A feasibility study," Radiology **226**, 897–905 (2003).
[15]E. Stewart *et al.*, "Focused ultrasound treatment of uterine fibroid tumors: Safety and feasibility of a noninvasive thermoablative technique," Am. J. Obstet. Gynecol. **189**, 48–54 (2003).
[16]R. F. Paterson, E. Barret, T. M. Siqueira, T. A. Gardner, J. Tavakkoli, V. V. Rao, N. T. Sanghvi, L. Cheng, and A. L. Shalhav, "Laparoscopic partial kidney ablation with high intensity focused ultrasound," J. Urol. **169**, 347–351 (2003).
[17]A. Okada, T. Murakami, K. Mikami, H. Onishi, N. Tanigawa, T. Marukawa, and H. Nakamura, "A case of hepatocellular carcinoma treated by MR-guided focused ultrasound ablation with respiratory gating," Magn. Reson. Med. Sci. **5**, 167–171 (2006).
[18]G. Vallancien, M. Harouni, B. Guillonneau, B. Veillon, and J. Bougaran, "Ablation of superficial bladder tumors with focused extracorporeal pyrotherapy," Urology **47**, 204–207 (1996).
[19]D. Gianfelice, C. Gupta, W. Kucharczyk, P. Bret, D. Havill, and M. Clemons, "Palliative treatment of painful bone metastases with MR imaging-guided focused ultrasound," Radiology **249**, 355–363 (2008).
[20]B. Liberman *et al.*, "Pain Palliation in patients with bone metastases using MR-guided focused ultrasound surgery: A multicenter study," Ann. Surg. Oncol. **16**, 140–146 (2008).
[21]K. Hynynen, G. Clement, N. McDannold, N. Vykhodtseva, R. King, P. White, S. Vitek, and F. Jolesz, "500-element ultrasound phased array system for noninvasive focal surgery of the brain: A preliminary rabbit study with ex vivo human skulls," Magn. Reson. Med. **52**, 100–107 (2004).
[22]K. Hynynen, N. McDannold, G. Clement, F. Jolesz, E. Zadicario, R. Killiany, T. Moore, and D. Rosen, "Pre-clinical testing of a phased array ultrasound system for MRI-guided noninvasive surgery of the brain—A primate study," Eur. J. Radiol. **59**, 149–156 (2006).
[23]K. Hynynen, "MRI-guided focused ultrasound treatments," Ultrasonics **50**, 221–229 (2010).
[24]S. Vaezy, X. Shi, R. Martin, E. Chi, P. Nelson, M. Bailey, and L. Crum, "Real-time visualization of high-intensity focused ultrasound treatment using ultrasound imaging," Ultrasound Med. Biol. **27**, 33–42 (2001).
[25]J. Tavakkoli and N. T. Sanghvi, "Ultrasound-guided HIFU and thermal ablation," in *Therapeutic Ultrasound: Mechanisms to Applications*, edited by V. Frenkel (Nova Science Publishers, Hauppauge, 2011), pp. 137–161.
[26]M. Xu and L. V. Wang, "Photoacoustic imaging in biomedicine," Rev. Sci. Instrum. **77**, 041101 (2006).
[27]T. Khokhlova, I. M. Pelivanov, O. A. Sapozhnikov, V. S. Solomatin, and A. A. Karabutov, "Opto-acoustic diagnostics of the thermal action of high-intensity focused ultrasound on biological tissues: The possibility of its applications and model experiments," Quantum Electron. **36**, 1097–1102 (2006).
[28]H. Cui and X. Yang, "Real-time monitoring of high-intensity focused ultrasound ablations with photoacoustic technique: An in vitro study," Med. Phys. **38**, 5345–5350 (2011).
[29]Y. Sun and B. O. Neill, "Imaging high-intensity focused ultrasound-induced tissue denaturation by multispectral photoacoustic method: An ex vivo study," Appl. Opt. **52**, 1764–1770 (2013).
[30]P. Chitnis, H. Brecht, R. Su, and A. Oraevsky, "Feasibility of optoacoustic visualization of high-intensity focused ultrasound-induced thermal lesions in live tissue," J. Biomed. Opt. **15**, 021313 (2010).
[31]K. Larin, I. Larina, and R. Esenaliev, "Monitoring of tissue coagulation during thermotherapy using optoacoustic technique," J. Phys. D: Appl. Phys. **38**, 2645–2653 (2005).
[32]M. Arsenault, M. Kolios, and W. Whelan, "Optoacoustic detection of thermal lesions," Proc. SPIE **7177**, 71771V (2009).
[33]J. Ritz, A. Roggan, C. Isbert, G. Muller, H. Buhr, and C. Germer, "Optical properties of native and coagulated porcine liver tissue between 400 and 2400 nm," Lasers Surg. Med. **29**, 205–212 (2001).
[34]A. M. K. Nilsson, C. Sturesson, D. L. Liu, and S. Andersson-Engels, "Changes in spectral shape of tissue optical properties in conjunction with laser-induced thermotherapy," Appl. Opt. **37**, 1256–1267 (1998).
[35]K. Ishii, A. Kimura, and K. Awazu, "Optical properties of tissues after laser treatments in the wavelength range of 350–1000 nm," Proc. SPIE **6991**, 69912F (2008).
[36]A. Yaroslavsky, P. Schulze, I. Yaroslavsky, R. Schober, F. Ulrich, and H.-J. Schwarzmaier, "Optical properties of selected native and coagulated human brain tissues in vitro in the visible and near infrared spectral range," Phys. Med. Biol. **47**, 2059–2073 (2002).
[37]B. Soroushian, W. M. Whelan, and M. C. Kolios, "Study of laser-induced thermoelastic deformation of native and coagulated ex-vivo bovine liver tissues for estimating their optical and thermomechanical properties," J. Biomed. Opt. **15**, 065002 (2010).
[38]B. Soroushian, W. M. Whelan, and M. C. Kolios, "Dynamics of laser induced thermoelastic expansion of native and coagulated ex-vivo soft tissue

samples and their optical and thermo- mechanical properties," Proc. SPIE **7899**, 78990Z (2011).
[39]S. Rahimian, *An Acoustic Backscatter-Based Method for Estimating Attenuation Towards Monitoring Lesion Formation in High Intensity Focused Ultrasound* (Ryerson University, 2012).
[40]E. Hysi, R. K. Saha, and M. C. Kolios, "Photoacoustic ultrasound spectroscopy for assessing red blood cell aggregation and oxygenation," J. Biomed. Opt. **17**(12), 125006 (2012).
[41]A. A. Oraevsky, S. L. Jacques, and F. K. Tittel, "Determination of tissue optical properties by piezoelectric detection of laser-induced stress waves," Proc. SPIE 1882, Laser-Tissue Interaction IV, 86 (July 7, 1993).
[42]V. E. Gusev and A. A. Karabutov, *Laser Optoacoustics* (American Institute of Physics, New York, 1992).
[43]Shimadzu Corporation, *Diffuse Reflectance Measurement* (2013).
[44]Shimadzu Corporation, *Transmittance Measurement* (2013).
[45]S. A. Prahl, M. J. C. van Gemert, and A. J. Welch, "Determining the optical properties of turbid media by using the adding-doubling method," Appl. Opt. **32**, 559–568 (1993).
[46]S. A. Prahl, Inverse Adding-Doubling program: Version 3–9–6 (http://omlc.ogi.edu/software/iad/index.html) (2013).
[47]D. A. Boas, J. P. Culver, J. J. Stott, and A. K. Dunn, "Three dimensional Monte Carlo code for photon migration through complex heterogeneous media including the adult human head," Opt. Exp. **10**, 159–170 (2002).
[48]G. Saiko, A. Pandya, I. Schelkanova, M. Sturmer, R. J. Beckert, and A. Douplik, "Optical detection of a capillary grid spatial pattern in epithelium by spatially resolved diffuse reflectance probe: Monte Carlo verification," IEEE J. Select. Top. Quantum Electron. **20**, 1–9 (2014).
[49]J. Swartling, S. Pålsson, P. Platonov, S. B. Olsson, and S. Andersson-Engels, "Changes in tissue optical properties due to radio-frequency ablation of myocardium," Med. Biol. Eng. Comput. **41**, 403–409 (2003).
[50]S. Rahimian and J. Tavakkoli, "Estimating dynamic changes of tissue attenuation coefficient during high-intensity focused ultrasound treatment," J. Ther. Ultrasound **14**, 1–22 (2013).
[51]N. Bush, I. Rivens, G. ter Haar, and J. Bamber, "Acoustic properties of lesions generated with an ultrasound therapy system," Ultrasound Med. Biol. **19**, 789–801 (1993).
[52]J. Barton, G. Frangineas, H. Pummer, and J. Black, "Cooperative phenomena in two-pulse, two-color laser photocoagulation of cutaneous blood vessels," Photochem. Photobiol. **73**, 642–650 (2001).
[53]M. Meinke, G. Müller, J. Helfmann, and M. Friebel, "Optical properties of platelets and blood plasma and their influence on the optical behavior of whole blood in the visible to near infrared wavelength range," J. Biomed. Opt. **12**, 014024 (2007).
[54]*Optical-Thermal Response of Laser-Irradiated Tissue*, 2nd ed., edited by A. Welch and M. van Gemert (Springer, New York, 2011).
[55]S. Thomsen, S. Jacques, and S. Flock, "Microscopic correlates of macroscopic optical property changes during thermal coagulation of myocardium," Proc. SPIE **1202**, 2–11 (1990).
[56]I. F. Cilesiz and A. J. Welch, "Light dosimetry: Effects of dehydration and thermal damage on the optical properties of the human aorta," Appl. Opt. **32**, 477–487 (1993).